Clutter Effects on Ground Moving Target Velocity Estimation with SAR Along-Track Interferometry

Shen Chiu
Space-Based Radar Group, Radar Systems Section
Defence R&D Canada - Ottawa, 3701 Carling Ave, Ottawa, ON, Canada, K1A 0Z4

***Abstract*— The SAR interferogram, defined as the product of the first channel and the complex conjugate of the second, is one way of comparing two SAR channels. When the two sub-apertures are aligned along the flight path, targets with non-zero radial velocities can be detected by exploiting the phase information of the interferogram. This paper examines the effect of clutter interference on the interferometric phase and provides a simple method for mitigating the clutter contamination by using time-frequency (TF) analysis techniques and a velocity-offset matched filter (VOMF). Both simulated and airborne results are presented.**

I. Introduction

The RADARSAT-2 (R2) design allows two portions of the full antenna aperture to be used independently with two separate receivers [1]. These two sub-apertures arranged to lie along the flight path enable one to detect targets with non-zero range and azimuth velocity components by providing essentially two identical views of the illuminated scene but at slightly different times. The application of the SAR along-track interferometry (ATI) to ground moving target indication (GMTI) has been previously investigated, e.g., [2], [3], [4].

It can be shown that a moving target having radial motion v_r causes a differential phase shift $\Delta\phi = 4\pi\delta t v_r/\lambda$, which may be detected by interferometric combination of the signals from the two channels. The interferometric phase $\Delta\phi$ is often used by authors to estimate the target's radial speed, e.g., [3], [4], [5]. This result, however, does not take into account the fact that the stationary clutter unavoidably corrupts the interferometric phase of the mover and, hence, does not always give the correct radial velocity of the target depending on its signal-to-clutter environment [6].

When a moving target's signal is SAR-processed, the imaged mover is azimuthally displaced according to its radial velocity and superimposed upon clutter at a wrong location. The target signal is, therefore, always contaminated with clutter power irrespective of the moving targets' physical dimensions relative to the spatial geometric resolution of the SAR. Thus, the resulting interferometric phase of the mover yields an erroneous estimate of the target's radial velocity, and the target's azimuth shift correction derived from the estimate is consequently erroneous as well.

In this paper, both simulated and airborne experimental data are examined in order to shed light on the nature of the contamination and to help to provide means of mitigating clutter effects on the target velocity estimation.

II. Simulation

Simulation experiments are carried out using deterministic point targets moving at the same range position during the observation time. The generated signals are assumed to be range-compressed with unity compression gain and without additive thermal noise or multiplicative phase noise. The received radar echoes from the fore (1) and aft (2) apertures can be described by

$$s_i(t) = \sum_{X,Y} a(t;X,Y)\sigma(X,Y)e^{-j\frac{4\pi}{\lambda}R_i(t;X,Y)}, \qquad (1)$$

where $a(t;X,Y)$ is the antenna pattern modulation, $\sigma(X,Y)$ is the radar backscatter coefficient, and $R_i(t;X,Y)$ is the distance from the radar's fore ($i = 1$) or aft ($i = 2$) aperture center to the target. The summation is over all targets at their initial azimuth-range positions (X,Y). We have also assumed that the two channels are balanced, i.e., $a_1(t;X,Y) = a_2(t;X,Y) = a(t;X,Y)$, and that $\sigma(X,Y)$ is the same for both apertures when the signals from the two channels are registered spatially.

When the radar transmits a sequence of pulses, $n = 1,2,3,\ldots,N$, with burst length T_{burst} at a pulse repetition interval T_{pri}, the total number of pulses transmitted is $N = T_{burst}/T_{pri} + 1$. By expressing "slow time" t in terms of n, (1) becomes

$$s_i(n) = \sum_{X,Y} a(-\frac{T_{burst}}{2} + (n-1)T_{pri};X,Y)\sigma(X,Y) \times e^{-j\frac{4\pi}{\lambda}R_i(-\frac{T_{burst}}{2}+(n-1)T_{pri};X,Y)}. \qquad (2)$$

Note that $t = 0$ is arbitrarily chosen to be at the center of the burst.

For simplicity, we use an airborne flat-earth geometry as shown in Fig. 1. For a ground moving target (i.e., $v_z = 0$) travelling in a straight line at a constant velocity (v_x, v_y), the slant range history from aperture 1 or 2 to the target is

$$R_i(t;X,Y) = \{[X + v_x t - v_a(t - t_{delay})]^2 + (Y + v_y t)^2 + H^2\}^{\frac{1}{2}}, \qquad (3)$$

where H is the platform altitude, and v_x and v_y are target's azimuth and ground range velocity components, respectively. To register the two SAR images spatially, channel 1 is delayed by $T_{delay} = -T_{pri}$, and for channel 2, $T_{delay} = 0$. Here it is

0-7803-7929-2/03/$17.00 (C) 2003 IEEE

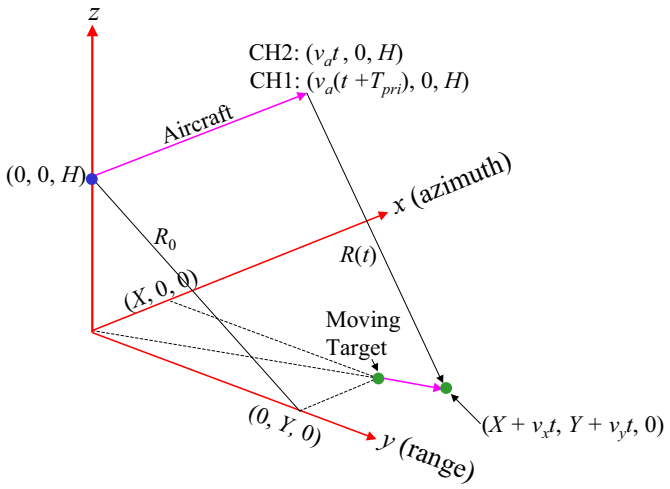

Fig. 1. Airborne geometry, showing aircraft and target positions at $t = 0$ and $t = T_{pri}$. The mover is assumed moving in a straight line at a constant velocity.

assumed that the distance d between the fore and aft aperture phase centers is equal to $v_a T_{pri}$.

We examine clutter interference by looking at the simpler problem of a stationary point target interfering with a moving point target by intentionally overlapping them in the SAR image. For the two targets at a same initial Y position, this is accomplished by positioning the mover

$$\Delta X = \frac{v_y v_a Y}{(v_x - v_a)^2 + v_y^2} \tag{4}$$

away from the stationary target in the x direction. The two targets then overlap in azimuth when the signals are SAR-processed. For instance, a mover with $v_y = -6$ m/s and $v_x = 0$ m/s, initially at $Y = 7948.67$ m, leads to an azimuth shift of -360.56 m. In order for a -6 m/s target to overlap in a SAR image with a stationary target at position $X = 0$, the mover must be initially at $X = +360.56$ m.

Before analyzing the simulation results, let us first examine analytically the clutter effect on a target's interferometric phase for deterministic signal and clutter. Let us assume, for simplicity, that two interfering point targets (one moving and one stationary) are perfectly compressed in the SAR image (an unlikely scenario, since a moving object is not well focussed by the stationary-terrain matched filter), then the moving target's signals received by the two sub-apertures (1 and 2) can be written as

$$\hat{s}_{1t} = A_{1t}\delta(y - Y_{1t})\delta(x - X_{1t})e^{j4\pi\frac{R'_{1t}}{\lambda}} \tag{5}$$

$$\hat{s}_{2t} = A_{2t}\delta(y - Y_{2t})\delta(x - X_{2t})e^{j4\pi\frac{R'_{2t}}{\lambda}} \tag{6}$$

and the stationary target's (or clutter's) signals as

$$\hat{s}_{1c} = A_{1c}\delta(y - Y_{1c})\delta(x - X_{1c})e^{j4\pi\frac{R'_{1c}}{\lambda}} \tag{7}$$

$$\hat{s}_{2c} = A_{2c}\delta(y - Y_{2c})\delta(x - X_{2c})e^{j4\pi\frac{R'_{2c}}{\lambda}} \tag{8}$$

where A combines the azimuth-compression gain and the backscatter coefficient, and R'_i is R_i modified by convolving with the stationary-world azimuth reference function.

When the moving target's impulse-response overlaps with that of the stationary clutter in a SAR resolution cell, they are added coherently (i.e. in magnitude and phase). For overlapping targets, $X_t = X_c$ and $Y_t = Y_c$, and $\delta(\bullet)$ can be set to 1 in equations (5) to (8). Therefore, when the two registered SAR images are combined to form an along-track interferogram, the resulting signal becomes

$$\begin{aligned} s_{ATI} &= (\hat{s}_{1t} + \hat{s}_{1c})(\hat{s}_{2t} + \hat{s}_{2c})^* \\ &= A_{1t}A_{2t}e^{j4\pi\frac{R'_{1t}-R'_{2t}}{\lambda}} + A_{1c}A_{2c}e^{j4\pi\frac{R'_{1c}-R'_{2c}}{\lambda}} \\ &\quad + A_{1t}A_{2c}e^{j4\pi\frac{R'_{1t}-R'_{2c}}{\lambda}} + A_{1c}A_{2t}e^{j4\pi\frac{R'_{1c}-R'_{2t}}{\lambda}}. \end{aligned} \tag{9}$$

The first term in (9) is the moving target's interferogram and its phase θ_{target} can be shown to be equal to

$$\theta_{target} = \frac{4\pi(R'_{1t} - R'_{2t})}{\lambda} = \frac{4\pi v_r T_{pri}}{\lambda}, \tag{10}$$

where v_r is the target's radial velocity with respect to the radar. The second term is the stationary clutter's interferogram and its phase should be equal to zero, since a stationary scene does not change with time and $R'_{1c} = R'_{2c} = R'_c$.

The third and fourth terms are cross terms, which come from the clutter contamination at the SAR image formation stage. Because of this interference, the multiplication of the contaminated signal from the fore channel with the conjugate of the signal from the aft channel leads to these undesirable cross terms. Since the phase angle is 2π periodic, the two cross terms may have very different phase values depending on R'_c, R'_{1t}, and R'_{2t}. This is especially true for real data in that many scatterers exist in a resolution cell with slightly different R_c, R_{1t}, and R_{2t} values. Therefore, the cross signals result in an ATI signal that is not easily predictable. Moreover, the targets' impulse responses are not real delta functions, specially for moving targets, which are poorly focused due to the unmatched azimuth filter. This leads to a point target's impulse response that overlaps with several neighboring resolution cells. The spreading also means a varying signal-to-clutter ratio (SCR) across the target's response, which in turn affects its ATI phase. This SCR dependence can be clearly seen in (9) and is discussed in detail elsewhere, e.g., [6], [7].

We first examine a case where a -6 m/s point mover at $X = +360.56$ m overlaps with stationary point target at $X = 0$ when the signals are SAR-processed. The ratio of mover's RCS to that of the stationary target is set at 6:1 (or 7.8 dB). This is necessary for the mover's impulse response to be at a level comparable to that of the stationary target when they are SAR-processed with a stationary-world assumption. Fig. 2 shows the output SAR signals from channel 1 for spatially non-overlapping and overlapping targets. Only the magnitude of the overlapping targets is shown (in red). The clutter interference changes the shape of the mover's impulse response; see Fig. 2. Its phase is also significantly changed by

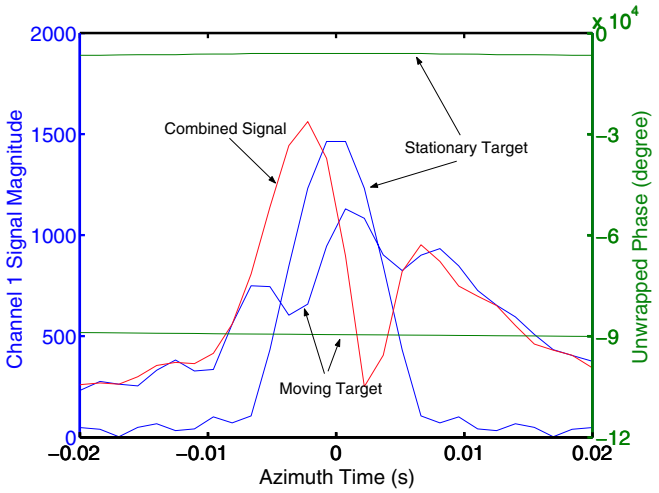

Fig. 2. Mover's and stationary target's SAR signals from channel 1 shown separately (blue: magnitude; green: phase) and combined (red: magnitude). $RCS_{target} : RCS_{clutter} = 6 : 1$

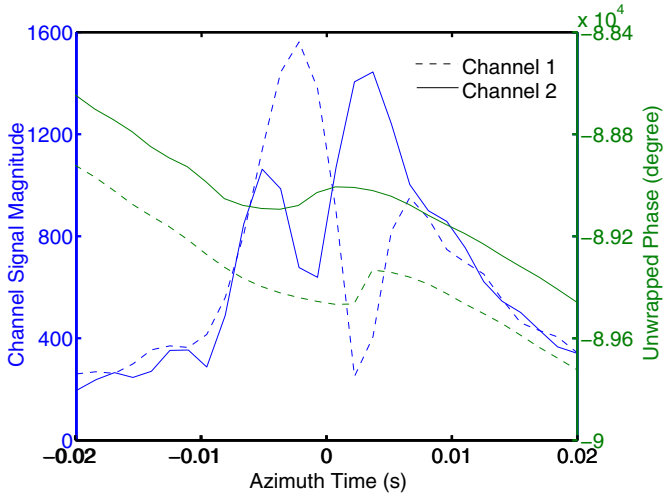

Fig. 3. Combined mover/stationary target's SAR signals from Channels 1 and 2. $RCS_{target} : RCS_{clutter} = 6 : 1$

the interference as can be seen in Fig. 3, where the combined SAR signal from channel 2 is also shown. Note the significant difference between channel 1 and channel 2.

When the two SAR images are combined to form an interferogram, as shown Fig. 4, the resulting magnitude and phase, which depend on various factors such as the degree of spatial overlap, SCR, and the mover's velocity, are clearly quite unpredictable. From Fig. 4 or 6(a), one sees that the phase of the interferogram can vary from -90^0 to $+90^0$. In fact, the ATI phase can have values outside the bounds of the stationary target's true ATI phase and that of the mover, which are supposedly 0^0 and 84.5^0, respectively. At first, one expects the combined ATI phase value (target plus clutter) to fall within these two bounds, but as we have examined earlier, the cross terms from (9) give rise to this peculiar behavior

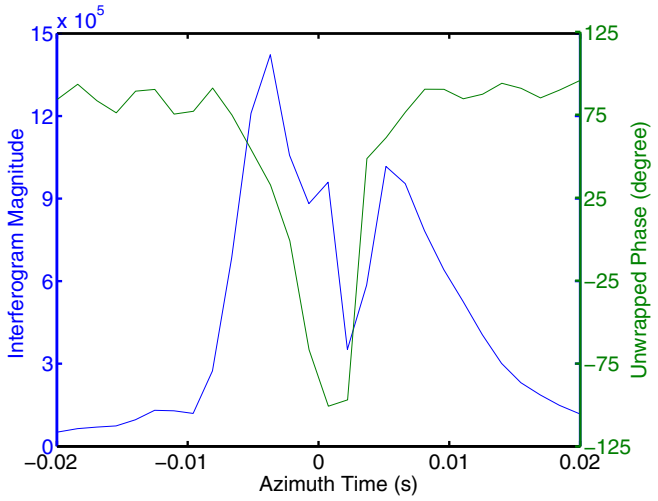

Fig. 4. SAR interferogram: the product of channel 1 SAR signal with the conjugate of channel 2 SAR signal. $RCS_{target} : RCS_{clutter} = 6 : 1$

of the interferogram. Note that the targets have no statistical distributions in both magnitude and phase nor additive thermal noise or multiplicative phase noise, therefore, the observed scatter in the ATI phase is purely a result of the interference of the two spatially overlapping targets.

In order to estimate the true velocity and position of a moving target, one must estimate the ATI phase from its uncorrupted signal; that is, one must somehow "sift out" the interfering clutter from the moving target's signal in order to obtain a "clean" target signal. Our proposed approach is to use time-frequency (TF) techniques to separate the mover from the stationary clutter. Fig. 5 shows how this signal "sifting" can be accomplished.

The range-compressed signal (but uncompressed in azimuth) from a range line containing a moving target buried in background clutter is represented in the time-frequency format. The green patch represents the stationary clutter, whose spectra are centered around zero Doppler because it has zero mean radial velocity. It has, however, a bandwidth because the radar has a finite beamwidth and also because the radar platform moves with respect to the stationary world. The moving point target is represented by the red sloped line with its Doppler centroid slightly shifted due to its non-zero radial velocity component.

As can be seen in Fig. 5, the target signals are completely buried in clutter in time but only partially in frequency, with a small portion of spectrum outside the clutter band. The proposed method uses short-time FFT to divide the "aperture time" into small time segments. Signals from most of these small time segments are contaminated with clutter, but a few of these time segments contain uncontaminated target signals, depending on the extend of band overlap (i.e., the target's radial velocity component). Clean target signals can then be obtained by choosing the appropriate time segments to compute the target's true ATI phase in frequency domain.

By applying this technique to the previous 6 m/s target

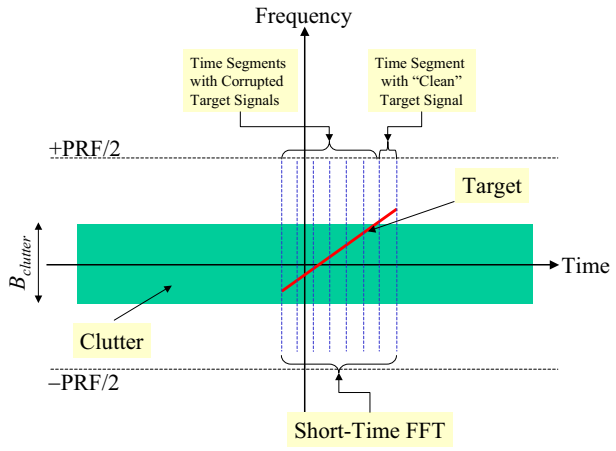

Fig. 5. TF representation of a range-compressed range line data containing a moving target signal "buried" in a stationary background clutter.

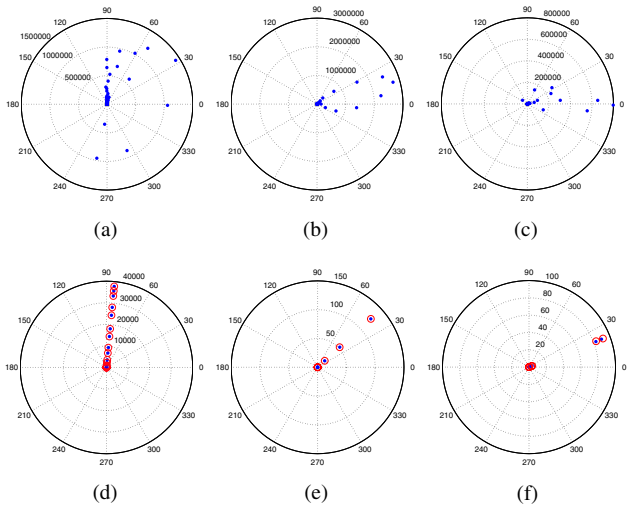

Fig. 6. (a) - (c) are "clutter"-corrupted ATI signals for targets with $v_y = -6, -3, -1.5$ m/s and RCS ratios 6:1, 1;1, and 1:1, respectively; (d) - (f) are targets' ATI signals after the TF filtering (shown in blue dots) and red circles are targets' true signals.

described above, one obtains the result as shown in Fig. 6(d). The blue solid dots are the TF "sifted" signal and the red circles are the target's true signal, shown here for comparison. The technique indeed gives the target's correct ATI phase. Other target velocities, $v_y = 3$ m/s and 1.5 m/s, were also tested, and the results before applying TF filtering are plotted in Figs. 6(b) and 6(c) and after the filtering in Figs 6(e) and 6(f). In each case, the TF sifting technique successfully yields the target's true ATI phase. One notes that this technique requires that there is a sizeable clutter-free region in the spectrum, where clean target signal can be extracted. Both the simulation and the airborne radar to be discussed in the next section have pulse repetition frequencies that significantly oversample (by 2.8) the azimuth data and, therefore, a large spectral region that is free of clutter is available for processing and for extracting clean target signals. In the case of Radarsat-2, however, the oversampling factor will be only 1.2, leaving only a very narrow clutter-free spectral region for extracting clean target phases. One other interfering factor that was not taken into account in this simulation study is the noise. The signal-to-noise ratio (SNR) is expected to be much smaller in this region because of the vanishing antenna pattern and a higher ATI phase noise. As demonstrated in the next section, the noise does interfere with the target signal, but in the airborne case it is not severe. For Radarsat-2, on the other hand, the noise is expected to be the major factor limiting the effectiveness of the proposed method. Not only that, the sidelobe could also be problematic in that if the target's signal is small in presumably the clutter-free region, the clutter contribution from sidelobes could also interfere with the target signal and, thus, making the task of ATI phase estimation more challenging.

III. Airborne Experiment

We now apply the same TF technique to real airborne data acquired by Environment Canada's CV580 C-band SAR configured in its along-track interferometer mode. Data were collected during an experiment conducted at Canadian Force Base Petawawa on 5 November 2000; see [8] for a more detailed description of the experimental site. Although controlled ground movers were used in the experiment, we will examine targets of opportunity (TOOs) on the highway (Hwy 17), which runs through the experimental site. The highway was monitored by two video cameras 600 m apart set up along a stretch of the highway to measure TOO speeds. The highway has a speed limit of 90 km/h, but most drivers drive 10-20 km/h over the speed limit. The video cameras monitored over 47 vehicles on the highway during the data acquisition period, and their monitored ground speeds varied from 83 km/h to 120 km/h, with an average speed of 102.6 km/h. The highway targets are analyzed instead of the controlled ones because all controlled targets were mounted with a corner reflector and this significantly increased their SCRs. We have indicated in the previous section [6] that clutter interference effect is sensitive to SCR and, therefore, the clutter effect will not be apparent when the SCR is large. Thus, targets of opportunity are more suitable for this type of study.

Over eight moving targets were detected using the so-called "Rare-Events" Detector developed by the author ([9], [10]) as shown in Fig. 7. These eight detected targets are labelled T1, T2, ..., T8 in the figure. The red squares are targets moving towards the radar and the green squares are those moving away from the radar.

Due to space limitation, we will only discuss the results obtained for T1, T2, and T8. The clutter-contaminated interferograms for these targets are plotted in polar format in Figs. 8(a) - 8(c). At first glance, the interferograms seem to show clutter contamination as their phases appear scattered without well defined values. One good indication of whether a target is contaminated or not is to see if its azimuth shift correction, derived from its estimated ATI phase, correctly puts

the target back to its true position. Fortunately, we know that these TOOs must be moving along the highway, therefore the azimuth shifts based on the ATI phase indicate the severity of the interference.

A target's radial velocity v_r is calculated from its estimated ATI phase θ using (10), and its azimuth shift correction ΔX is, in turn, computed from v_r using

$$\Delta X = R\frac{v_r}{v_a} = R\frac{\theta\lambda}{4\pi T_{dpca} v_a}, \qquad (11)$$

where $T_{dpca} = d/v_a$ and d is the distance between the two phase centers of the fore and aft apertures.

Fig. 9 shows SAR-ATI images of the three targets under consideration. The white circles show shifted targets before azimuth correction. Green solid squares indicate corrected positions based on clutter-contaminated ATI phases. Red triangles are estimated positions according to the TF filtering technique as described in Sec. II. For comparison, we have also included estimated positions obtained using a velocity-offset matched filtering approach (VOMF), and they are shown as white triangles. This technique uses a matched filter with a velocity-offset v_y incorporated into its reference function. The v_y was chosen to be ± 9 m/s depending on the direction of the mover. This allows the matched filter integrate only the signal energy outside the clutter band and, thus, like the TF approach, permits a "clean" target signal to be extracted for computing the ATI phase. The VOMF technique is only feasible for the case where the azimuth data is significantly oversampled, as in the airborne case, so that the VOMF integrates only the target energy that is outside the clutter spectral band. For Radarsat-2, most of the target energy will be either in or folded back into the clutter band because the data is only oversampled by a factor of 1.2. Therefore, it is not possible for the VOMF to extract "clean" target energy from a mostly clutter-corrupted signal, when only a small clutter-free region is available. The

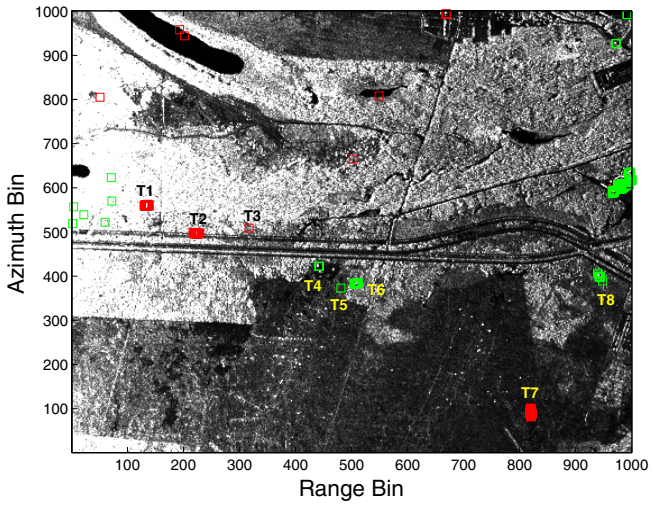

Fig. 7. Petawawa experimental site showing detected targets as □; red represents targets approaching radar and green moving away from radar.

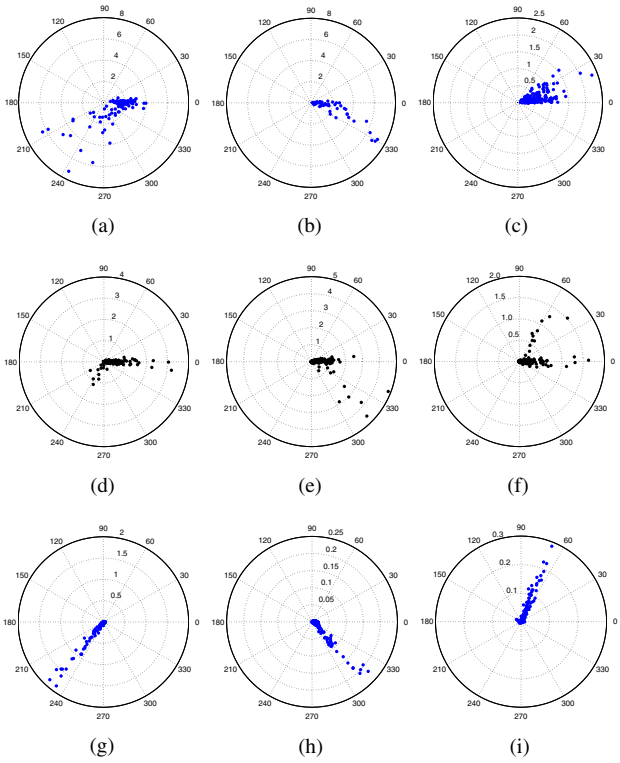

Fig. 8. (a) - (c) targets' corrupted ATI signals for T1, T2, and T8; (d) - (f) targets' ATI signals after TF filtering; (g) - (i) targets' ATI signals processed with a ± 9 m/s VOMF.

TF method, on the other hand, is capable of selecting a small frequency segment (or a time segment) that is free of clutter for extracting a clean target ATI phase.

For T1, the estimated target position, based on its contaminated ATI phase [Fig. 8(a)], puts the target more or less on the road; see Fig. 9(a). Even though its ATI phase is spread from -90^0 to -150^0, its average value (-125^0) correctly gives the target azimuth position. Since the target is moving almost directly towards the radar, its radial velocity v_r is high, and the ATI phase angle is expected to wrap around 2π, which occurs at $v_r = 13.15$ m/s (47.33 km/h). In fact, the measured ATI phases for all three targets under consideration must be unwrapped to yield target speeds that fall within the monitored speed range (83 to 120 km/h). For instance, T1's -125^0 phase is in fact $+595^0$, which yields a $v_r = +78.23$ km/h, or a ground velocity of $+107.42$ km/h after taking into account the imaging geometry. The TF method also correctly puts the target on the road, based on the estimated ATI phase of -120^0; see Figs. 8(d) and 9(a). This phase angle, after unwrapping, yields a ground velocity of $+108.32$ km/h. The VOMF approach, however, puts the target slightly off the road with an estimated ground velocity of $+106.51$ km/h.

The clutter contamination effects are more apparent in the cases of T2 and T8. For T2, its corrupted ATI phase [-28^0, Fig. 8(b)] yields a target position that is almost 50 meters off the road [see Fig. 9(a)] with an estimated ground velocity of $+121.4$ km/h. The TF and VOMF methods, on the other

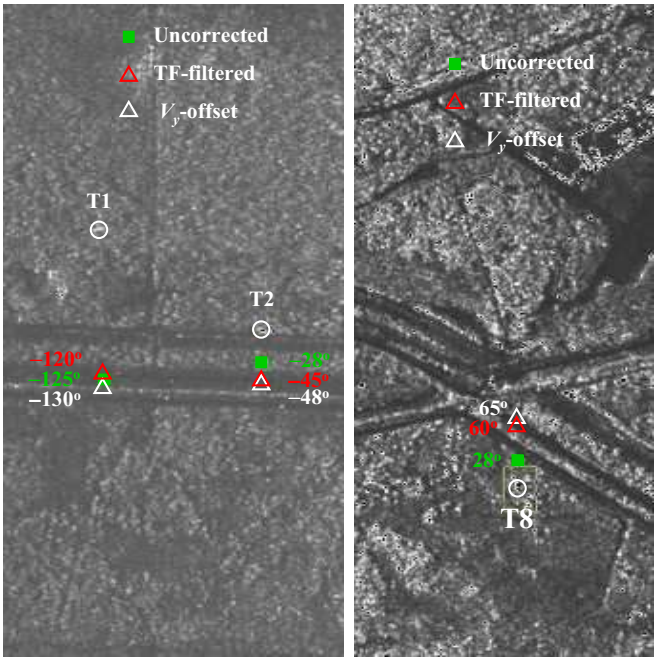

(a) (b)

Fig. 9. SAR-ATI images of three targets (T1, T2, and T8) under consideration. The circles show targets' shifted positions before azimuth corrections. Green solid squares indicate targets' corrected positions based on clutter-contaminated ATI phases. Red triangles are targets' estimated positions according to the TF filtering technique. For comparison, targets' estimated positions based on the VOMF approach are shown as white triangles.

hand, yield correct azimuth positions [Fig. 9(a)] with estimated ground speeds of $+118.43$ km/h [Fig. 8(e)] and $+117.9$ km/h [Fig. 8(h)], respectively. Similarly for T3, the clutter-corrupted ATI phase [$+28^0$, Fig. 8(c)] of the target does not correctly position the target on the highway; see Fig. 9(b). It is off by about 127 meters (i.e., off by 34.5^0). The estimated ground velocity is -122.1 km/h. Again, the results from the TF and VOMF methods agree reasonably well giving ATI phases of 60^0 [Figs. 8(f)] and 65^0 [Fig. 8(i)], respectively. The target is also correctly positioned on the highway within the image resolution. The estimated ground velocities are $+116.4$ km/h for the TF method and $+115.2$ km/h for the VOMF.

The reason that T2 and T8 are more seriously affected by the interfering clutter is that they have smaller ATI phases than T1, meaning that these targets are buried in the clutter band to a greater degree than T1 [11].

IV. Conclusions

We have examined the interference between stationary clutter and moving target in the SAR interferogram and discussed the implications on estimating moving target velocity and position with the ATI phase. A corrupted ATI phase leads to erroneous azimuth-position and radial-velocity estimation. It was shown that targets with smaller nominal ATI phases (i.e., before phase unwrapping) are more severely affected by the interfering clutter than targets with larger ATI phases. This is attributed to the extent of their spectral overlap with the clutter band. By using both time-frequency and velocity-offset matched filtering techniques, corrupted ATI phases were "cleaned up" and correct target positions were obtained for both simulated and airborne data. These techniques require that a clutter-free spectral region exists for processing. However, the TF approach is expected to be less sensitive to this limitation than the VOMF. The limitation is of concern to Radarsat-2 because of its small azimuth oversampling factor.

References

[1] A. A. Thompson, A. P. Luscombe, K. James, and P. Fox, "New modes and techniques of the RADARSAT-2 SAR," in *Proc. of IGARSS '01*, Sydney, Australia, July 2001.

[2] A. Moccia and G. Rufino, "Spaceborne along-track SAR interferometry: Performance analysis and mission scenarios," *IEEE Transactions on Aerospace and Electronic Systems*, vol. 37, pp. 199–213, 2001.

[3] M. Soumekh, "Moving target detection in foliage using along-track monopulse synthetic aperture radar imaging," *IEEE Transactions on Image Processing*, vol. 6, pp. 1148–1163, 1997.

[4] E. F. Stockburger and D. N. Held, "Interferometric moving ground target imaging," in *1995 IEEE international radar conference*, 1995, pp. 438–443.

[5] S. Barbarossa, "Detection and imaging of moving objects with SAR - Part I: Optimal detection and parameter estimation," *IEE Proceedings, Part F*, vol. 138, no. 2, pp. 79–87, February 1992.

[6] C. H. Gierull, "Moving target detection with along-track SAR interferometry," Technical Report TR 2002-084, Defence Research and Development Canada, August 2002.

[7] C. E. Gierull, R.and Livingstone, *The Applications of Space-Time Processing*, chapter SAR GMTI concept for RADARSAT-2, IEE Publishers, 2003.

[8] C.E. Livingstone, I. Sikaneta, C.H. Gierull, S. Chiu, A. Beaudoin, J. Campbell, J. Beaudoin, S. Gong, and T.A. Knight, "An airborne synthetic aperture radar (SAR) experiment to support RADARSAT-2 ground moving target indication (GMTI)," *Can. J. Rem. Sens.*, vol. 28, no. 6, pp. 1–20, 2002.

[9] S. Chiu, "Along-track interferometric SAR processing for RADARSAT-2 ground moving target indication," in *Proc. of the 4th IASTED International Conference on Signal and Image Processing*, Kaua'i, Hawaii, USA, August 2002, pp. 43–48.

[10] S. Chiu, "SAR along-track interferometry with application to RADARSAT-2 ground moving target indication," in *Proc. of SPIE on Image and Signal Processing for Remote Sensing VIII*, Crete, Greece, September 2002, pp. 246–255.

[11] C. H. Gierull and I. Sikaneta, "Raw data based two-aperture SAR-GMTI ground moving target indication," in *this proceeding, IGARSS '03*, Toulouse, France, July 2003.